Smart Materials in Medicine 1 (2020) 24–31

Contents lists available at ScienceDirect

Smart Materials in Medicine

journal homepage: www.keaipublishing.com/en/journals/smart-materials-in-medicine/

Review Article

Intramolecular motion-associated biomaterials for image-guided cancer surgery

Chao Chen [a], Youhong Tang [b,c], Dan Ding [a,*]

[a] State Key Laboratory of Medicinal Chemical Biology, Key Laboratory of Bioactive Materials, Ministry of Education, And College of Life Sciences, Nankai University, Tianjin, 300071, China
[b] Medical Device Research Institute, College of Science and Engineering, Flinders University, South Australia, 5042, Australia
[c] Institute for Nanoscale Science and Technology, College of Science and Engineering, Flinders University, South Australia, 5042, Australia

ARTICLE INFO

Keywords:
iMAB
Imaging guidance
Photophysical property
Intramolecular motions
Intermolecular interactions

ABSTRACT

Intramolecular motion-associated biomaterials (iMAB) are developing rapidly in the field of image-guided cancer surgery by virtue of their easily regulated photophysical property. Through manipulating the energy distribution after absorption of light, we can easily control the maximal energy decay of iMAB through radiative pathway or non-radiative pathway for optimized fluorescence guidance or promoted photoacoustic imaging guidance. Therefore, iMAB provide an opportunity to utilize the maximum potential of imaging reagents for precise guidance of cancer surgery. In this short review, recent progress in this field has been summarized and discussed to illuminate the design and regulation principles of iMAB for advanced precise cancer surgery.

1. Introduction

At present, comparing with other series of treatments, such as chemo/radio therapy, targeted therapy, immunotherapy and so on, cancer resection surgery is still the preferred and most commonly used strategy, especially when patients in the early stages [1–3]. However, in most cases, surgeons have to identify the tumor boundaries and the mini residue nodules hiding in surrounding tissues with naked eyes during the operation, which easily leads to the postoperative recurrence and irreversible damage to normal tissues. Therefore, precisely intraoperative cancer resection in the aid of optical imaging guidance holds great potential to address these severe problems, owing to its ultrahigh sensitivity and contrast, real-time modality, super temporal resolution and good biosafety [4–7]. With the help of imaging guidance, the boundaries between tumorous and normal tissues are able to be determined clearly, as well as the tiny nodules in the surrounding tissues, especially tiny ones (diameter < 1 mm) [8–15]. Thus, it tremendously promotes the postoperative survival rate by precise resection.

Along with the wide application of imaging guidance, optimized imaging performance is desired. Therefore, development of optical agents with longer excitation/emssion wavelength and higher brightness for fluorescence bioimaging and stronger heat production reagents provides the opportunity to address the issue. In fact, according to the rules elucidated by Jablonski diagram, there is a closely relevant relationship between the three energy pathways of optical agents at excited state and phototheranostics: 1) radiative pathway for fluorescence imaging; 2) non-radiative decay by thermo generation for photoacoustic imaging and photothermal therapy; 3) intersystem crossing process to generate ROS or phosphorescence for photodynamic therapy or phosphorescence imaging [27,31]. Obviously, radiative pathway and non-radiative decay are competitive. Therefore, it is a challenge to concentrate the absorbed energy of optical molecules to each pathway maximally. With the rapid development of this field, many kinds of optical imaging agents have emerged to promote the performance of imaging guidance, such as inorganic quantum dots, uponverting nanometerials, carbon materials, semiconducting polymers, small organic molecules and so on [22–25]. However, how to utilize the absorbed energy maximally to achieve the better imaging performance is still unresolved well.

Very recently, intramolecular motion-associated biomaterials defined as materials with rich intramolecular motion units (e.g., molecular rotor) for bioapplications have been developing rapidly in optical diagnosis and treatment, owing to its easily optimal imaging performance by regulating the photophysical property [26–30]. According to different energy distribution at excited state, iMAB are divided into two categories: biomaterials of enhanced radiative decay for PA imaging and biomaterials with optimized non-radiative pathway for fluorescence imaging or ROS generation. By regulation of photophysical property, iMAB realize the optimal energy distribution, thus could maximally concentrate the

* Corresponding author.
E-mail address: dingd@nankai.edu.cn (D. Ding).

https://doi.org/10.1016/j.smaim.2020.05.001
Received 24 March 2020; Received in revised form 18 May 2020; Accepted 20 May 2020
Available online 24 June 2020

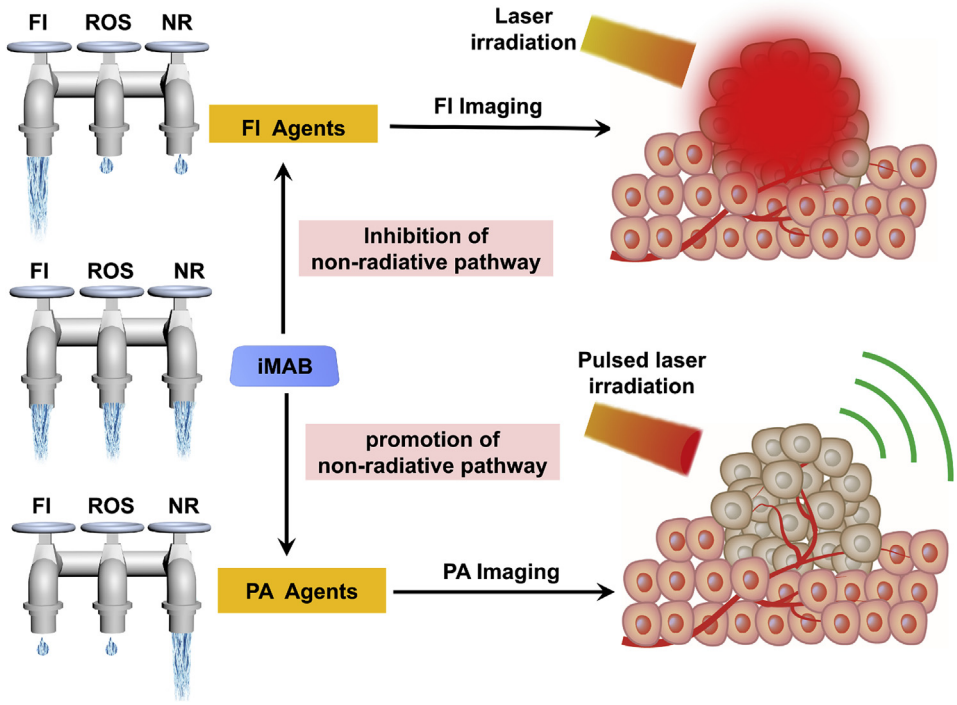

Scheme. 1. The schematic of cancer imaging guidance using iMAB by regulation of the photophysical property. FI: fluorescence, NR: non-radiation.

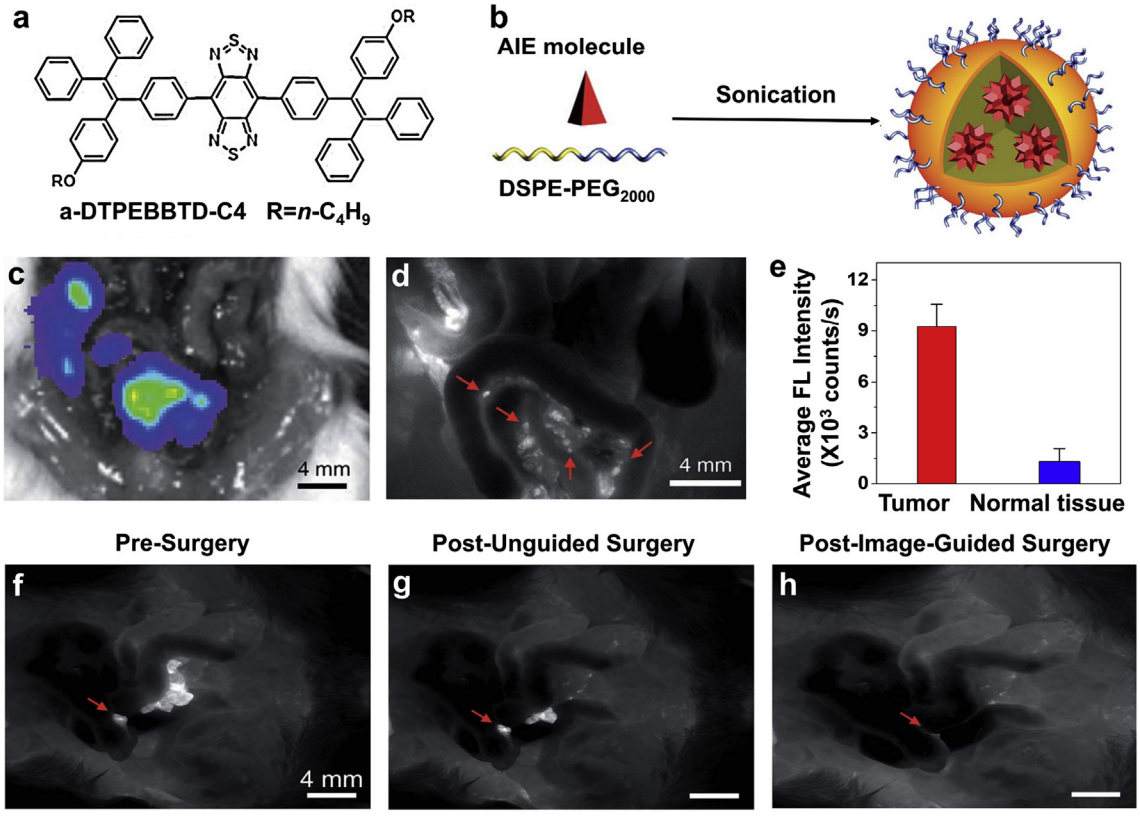

Fig. 1. (a) Chemical structure of a-DTPEBBTD-C4. (b) Schematic of the nanoprobe preparation. (c) Bioluminescence, and (d) fluorescence images collected from the mice of peritoneal metastases by intravenous administration of AIE NPs for 24 h. (e) Quantitative analysis of average fluorescence intensity from tumorous and normal tissues after intravenous administration of AIE NPs for 24 h. (f) Typical fluorescence image before resection. (g) Typical fluorescence images of the mice after resection with naked eyes and (h) after re-resection in the guidance of AIE NPs. (a–h) Adapted with permission from ref 9. Copyright 2017, The Royal Society of Chemistry.

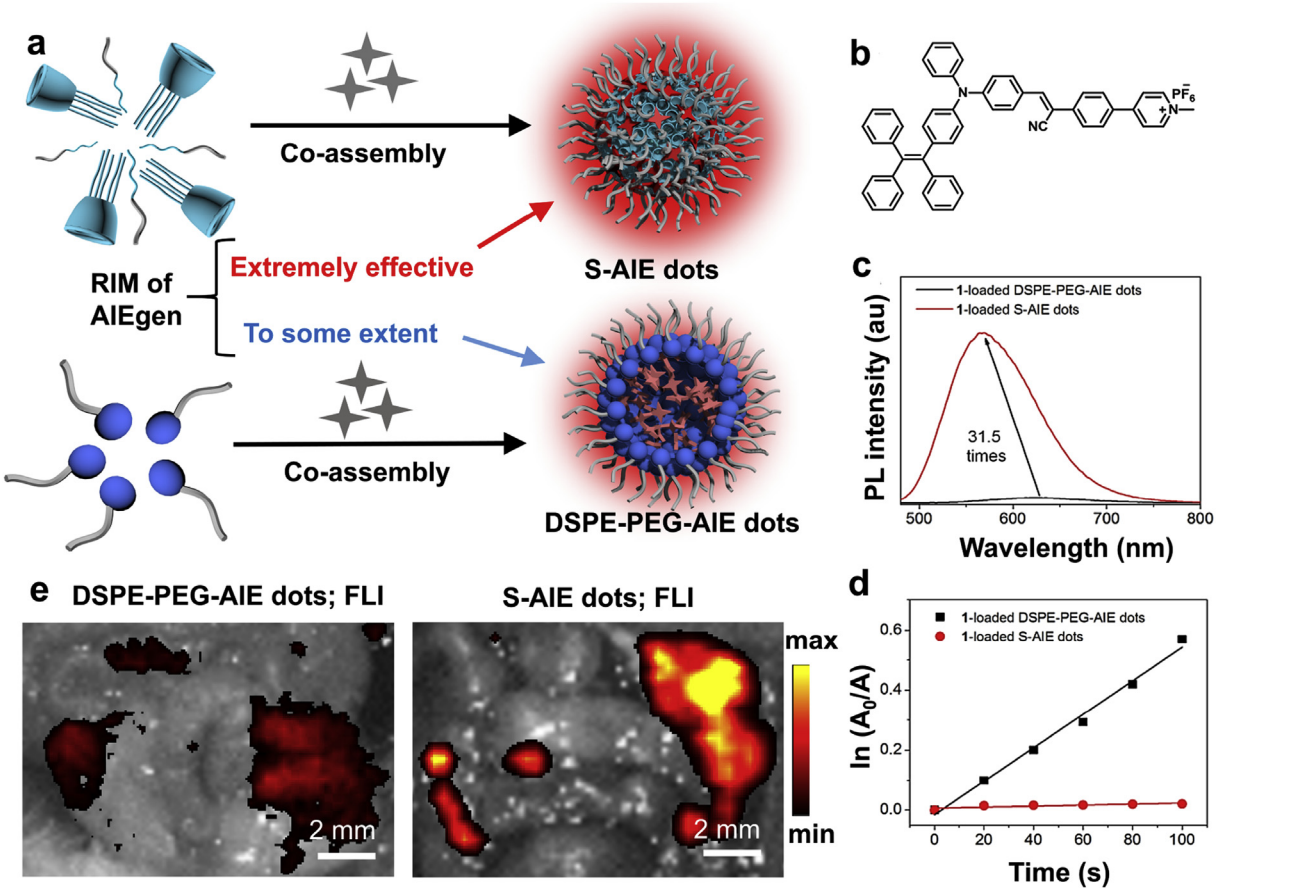

Fig. 2. (a) Schematic of preparation of S-AIE dots and DSPE-PEG-AIE dots. (b) Chemical structures of AIE molecules. (c) PL spectra and (d) plot of ROS production of S-AIE dots and DSPE-PEG-AIE dots in water. (e) Representative fluorescence images of the mice with peritoneal metastases after intravenous injection of DSPE-PEG-AIE dots and S-AIE dots for 24 h, respectively. (a–e) Adapted with permission from ref 11. Copyright 2020, Wiley-VCH.

absorbed energy to radiative pathway, non-radiative decay or ROS/-phosphorescence generation through intersystem crossing (ISC) according to our demands. Thereby, we can obtain the ultra-bright fluorescence agents by inhibiting the non-radiative dissipation (limitation of the intramolecular motions and intermolecular interactions) and ISC at the very highest level, leading to the absorbed energy maximally flow to the radiative pathway, while receiving super photoacoustic agents via facilitating the non-radiative decay by promoting the intramolecular motions (Scheme 1) [11,19,20]. Besides, incorporation of iMAB with other materials into nanoparticles also represents an emerging nano-engineering method for realizing better image-guided performance [10–12]. For instance, once incorporation of planer optical agents with iMAB within nanoparticles, much better imaging performance can be achieved. This is because the twisted structure of iMAB can strongly break up the intermolecular interactions (such as π-π stacking), which tremendously inhibit the non-radiative dissipation and ultimately benefit the radiative pathway [12]. In other cases, optimally multi-modal imaging property integrated in a single iMAB molecule endows the imaging guidance with a more personalized precision therapy [21,31].

Although image-guided cancer surgery using iMAB is increasing rapidly, there is scarcely any review article to summarize and generalize this emerging and promising field. In this short review, we concluded the recent progress in the field of image-guided cancer surgery using iMAB and elucidated the elaborate design and regulation principles of iMAB to maximally optimize the image-guided performance.

2. AIE based NIR image-guided surgery

Taking advantages of ultrahigh sensitivity and contrast, fluorescence imaging technique has been widely applied in the intraoperatively precise cancer resection [32–34]. In order to achieve better imaging performance, much efforts have been concentrated on these two aspects: 1) improving the excitation and emission wavelength of imaging agents to near-infrared (NIR) regions (700–1700 nm) to minimize the tissue autofluorescence and increase the penetration depth, and 2) promoting the brightness of optical agents to realize the ultrahigh sensitivity [9,11,28,35,36]. According to the rules of Jablonski diagram, radiative pathway and non-radiative decay are competitive. By inhibiting the non-radiative pathway or both non-radiative attenuation and ISC process, the optimal performance of fluorescence imaging could be achieved.

In the field of NIR imaging guidance, both organic and inorganic materials have been widely applied and proved to be successful [51]. Inorganic imaging agents (e.g., gold nanomaterials and upconverting nanoparticles) exhibit unique advantages in visualization of physiological and pathological process due to good stability, NIR absorption, adjustable imaging properties and multi-modal imaging ability [52]. Alternatively, organic imaging agents represent the other big category of NIR imaging guidance and disease diagnosis by virtue of excellent biosafety, high quantum yeild, large stokes shifts and flexible structures and so on [53]. However, traditional organic NIR fluorescent agents face challenges of fluorescence quench within aggregates, namely, aggregation-caused quenching (ACQ) effect, owing to their large plane structures to enhance molecular absorption. Thus, the reliability, precision and sensitivity of fluorescence imaging are damaged [37–40].

In contrast, the emergence of aggregation-induced emission (AIE) brings new opportunities for optimal bioimaging. AIE is the phenomenon that no emission or weak emission in dissolved state of optical molecules

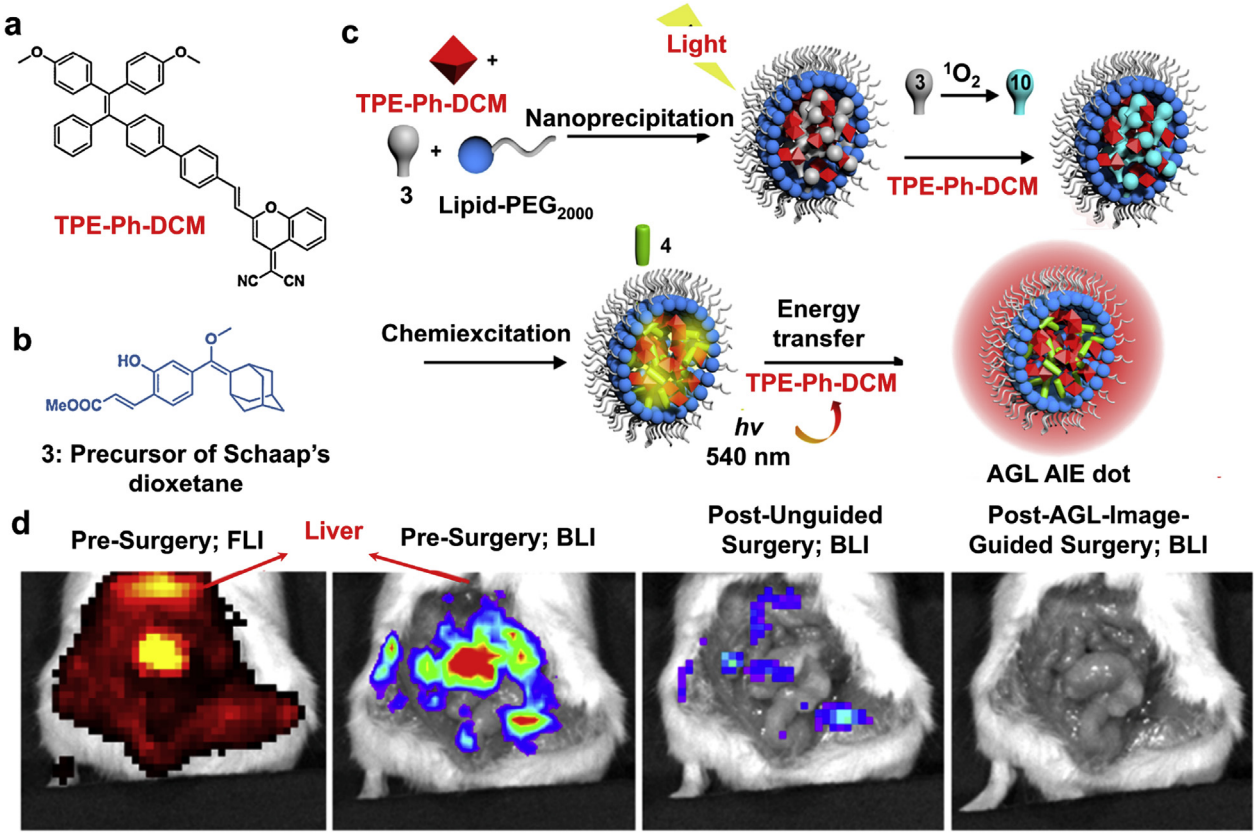

Fig. 3. (a) Chemical structures of TPE-Ph-DCM and (b) precursor of Schaap's dioxetane. (c) Schematic of achieving NIR afterglow luminescence of AGL-AIE dots. (d) Representative fluorescence and afterglow images of pre-surgery after intravenous injection of AGL-AIE dots for 2 h. Representative afterglow images of the mice with peritoneal metastases after unguided surgery and after re-operation guided by AGL-AIE dots. (a–d) Adapted with permission from ref 12. Copyright 2018, American Chemical Society.

due to strong intramolecular motion at excited state (non-radiative decay), but strong emssion in aggregated state as restriction of intramolecular motion (radiative pathway) [38–40]. Thereby, AIE molecules confer the potential of imaging agents to achieve optimal imaging performance by regulation of photophysical properties. For instance, Liu, Ding and co-workers designed a series of NIR molecules that combined tetraphenylethene (TPE) groups characterized by rich intramolecular motion units with benzo [1,2-*c*:4,5-*c*'] bis ([1,2,5] thiadiazole) (BBTD, a strong electron acceptor) [9]. In order to further weaken the non-radiative attenuation and increase fluorescence dissipation through destroying the intermolecular interactions (e.g., π-π stacking), different lengths and positions of alkyl chains were also introduced into the side of TPE groups (Fig. 1a). By this smart design, series of NIR molecules with AIE characteristic were synthesized and encapsulated into nanoparticles using DSPE-PEG_{2000} (Fig. 1b). As expected, a high quantum yield (QY = 5%) and long wavelength emission (maximum at 815 nm) NIR dot was achieved through restriction of intramolecular motions and intermolecular interactions (both of them can inhibit the non-radiative pathway).

Encouraged by the excellent fluorescence performance, Liu, Ding and co-workers applied these NIR dots in the guidance of precise cancer surgery using a mouse model of peritoneal carcinomatosis. In vivo imaging experiments demonstrate that NIR dots can specifically accumulate in peritoneal tumor nodules by intravenous injection (Fig. 1d). Meanwhile, the fluorescence intensity ratio of tumorous tissues to normal tissues reached 7.2, which 1.5-fold higher than the value of Rose criterion (Fig. 1e), owing to the high QY and NIR emission. Remarkably, with the help of NIR fluorescence guidance, tumor margins and nodules were clearly identified and precisely removed, especially for tiny ones (length <1 mm). In contrast, some tiny nodules were easy to escape from the naked eyes without NIR imaging guidance (Fig. 1g). Analogously, Tang and colleagues also designed a highly bright NIR-II molecule (maximum emission wavelength at 1030 nm, QY = 11%) by tuning the intramolecular motions and intermolecular interactions for intraoperative guidance of ureter [41]. Therefore, regulation of the intramolecular motions and intermolecular interactions (non-radiative pathway) by molecular design represent a promising method to improve the NIR-emissive brightness for optimized surgery guidance.

Despite the smart molecular design, nanoengineering that integrated several ingredients within a nanoparticle is another option, which skips the complex conjugation chemistry and realizes optimal phototheranostics [10,11,42,43]. Due to the great potential of iMAB to optimize the imaging behaviors by regulation of intramolecular motions, incorporation of components that can provide steric hindrance or interactions within nanoparticles holds great potential to improve the iMAB imaging performance [10,11]. As the competitive relationship among the three energy dissipation routes, the fluorescence and ROS generation (through ISC process) were significantly increased by inhibition of the non-radiative decay derived from intramolecular motions. Based on this principle, Tang, Ding and co-workers fabricated a combined nanodot, in which corannulene effectively inhibited the intramolecular motions of AIE (a classical iMAB). Compared with the DSPE-PEG encapsulated AIE dots, the levels of QY and ROS generation were enhanced 4.0-fold and 5.4-fold in corannulene-incorporated AIE dots, respectively, which promoted the cancer phototheranostics [10].

According to the theory of Jablonski diagram, it is obvious that simultaneous inhibition the non-radiative decay and ISC can maximize the energy flow to the radiative pathway, thus can extremely enhance the fluorescent brightness for imaging guidance. Based on this principle, Ding and colleagues prepared an ultrabright AIE dot with highly suppressed both non-radiative decay and ISC pathway by incorporation of

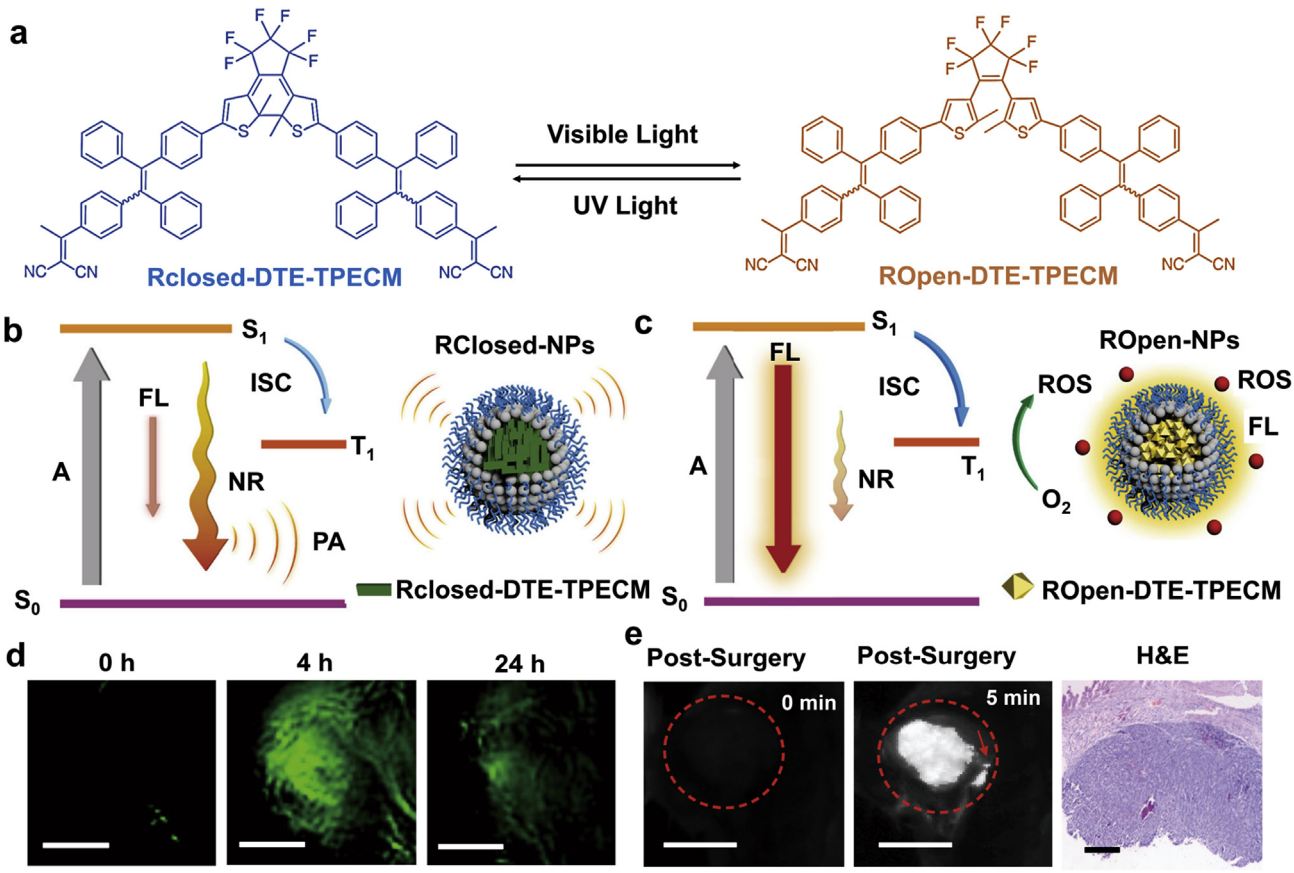

Fig. 4. (a) Chemical structure and light-driven transferability of DTE-TPECM molecules. (b–c) Illustration of the changes in photophysical processes of DTE-TPECM based NPs triggered by UV/visible irradiation. A: absorption, FL: fluorescence, NR: non-radiation, ISC: intersystem crossing. (d) Representative PA images after iv injection of Rclosed-YSA-NPs at different time points. (e) Representative fluorescence images of post-surgery before and after red light irradiation, and H&E analysis of resection site. (a–e) Adapted with permission from ref 31. Copyright 2018, Springer Nature.

calixarene for image-guided cancer surgery [11]. Calixarene is one of the most emerging supermolecules in kinds of macrocyclic hosts, shows great potential for developing biomedical nanomaterials due to its good biosafety and controllable host-guest interactions. They first synthesized a series of red-emissive agents with rich intramolecular motion units (Fig. 2a), which were followed by preparation of nanoparticles incorporated with carboxylic acid-modified calix [5]arene pentadodecyl ether (CC5A-12C), namely S-AIE dots. Compared with the AIE dots using DSPE-PEG as matrix, the fluorescence intensities of S-AIE dots were significantly increased by fabrication of CC5A-12C (maximum increase was 31.5 times, QY = 0.72), while the ROS production were sharply reduced to almost undetectable level (Fig. 2c). This result together with no phosphorescence of S-AIE dots in room temperature, indicated that ISC pathway was almost completely suppressed in S-AIE dots (Fig. 2d). Subsequently, fluorescence anisotropy study was conducted in this work to evaluate the confined nano-environment using 1,6-diphenyl-1,3,5-hexatriene (DPH), whose fluorescence anisotropy value would increase as the viscosity increased in the environment. From the study, the value of fluorescence anisotropy reached at 0.392 in S-AIE dots, which is very close to the maximum value of 0.395, and 1.8-fold higher than that of DSPE-PEG-AIE dots. Furthermore, when the S-AIE dots were frozen in liquid nitrogen, no significant increase of fluorescence intensity was observed in comparison with its solution in room temperature. These results demonstrated that intramolecular motions in S-AIE dots were thoroughly restricted and non-radiative decay was maximally inhibited. Emboldened by the success of maximally optimized fluorescence performance through both inhibition of non-radiative decay and ISC pathway. Ding et al. applied S-AIE dots in the guidance of cancer surgery using mouse models with peritoneal tumor metastases. The ultrahigh brightness of S-AIE dots promoted the precise visualization of metastases with ultra-sensitivity (SBR = 48.5, the highest in this field) and improved the postoperative survival rate (Fig. 2f-g).

3. Afterglow image-guided surgery

Afterglow luminescence has attracted great attention in bioimaging due to the persistent emission without excitation, ultrahigh sensitivity and deep tissue penetration [12,17,18]. However, excellent afterglow agents that can be used in phototheranostics are relative few, especially for organic materials. MEHPPV (poly[2-methoxy-5-(2-ethylhexyloxy)-1,4-phenylenevinylene]) is a good representative of polymeric afterglow agents applied in vivo diagnosis [44,45]. Another kind of promisingly small molecules are Schaap's dioxetanes, which can be easily designed to be biomarker-responsive and emission at different wavelengths [46,47]. Shabat and co-workers reported a series of compounds based on Schaap's dioxetanes, some of which reached at red emission but hardly to achieve imaging guidance due to the limited afterglow efficiency. To address the challenge, Ding and colleagues developed a NIR afterglow luminescent nanoprobe (AGL-AIE dot) that integrated by twisted AIEgens (a classic iMAB) and Schaap's dioxetanes together [12]. AGL-AIE dots obtained an outstanding luminescent efficiency in NIR regions (>650 nm) and realized ultralong luminescence times (more than 10 days) due to decreased intermolecular interactions and effective energy transfer to NIR AIEgens within nanoprobes (Fig. 3a–c). They further synthesized an ACQ compound without intramolecular motion units (TPE groups), followed by preparation of nanoprobes together with Schaap's dioxetanes, named ACL-ACQ dots. As shown in Fig. 3d, the afterglow intensity of AGL-ACQ dots was dramatically decreased in comparison to that of AGL-AIE dots,

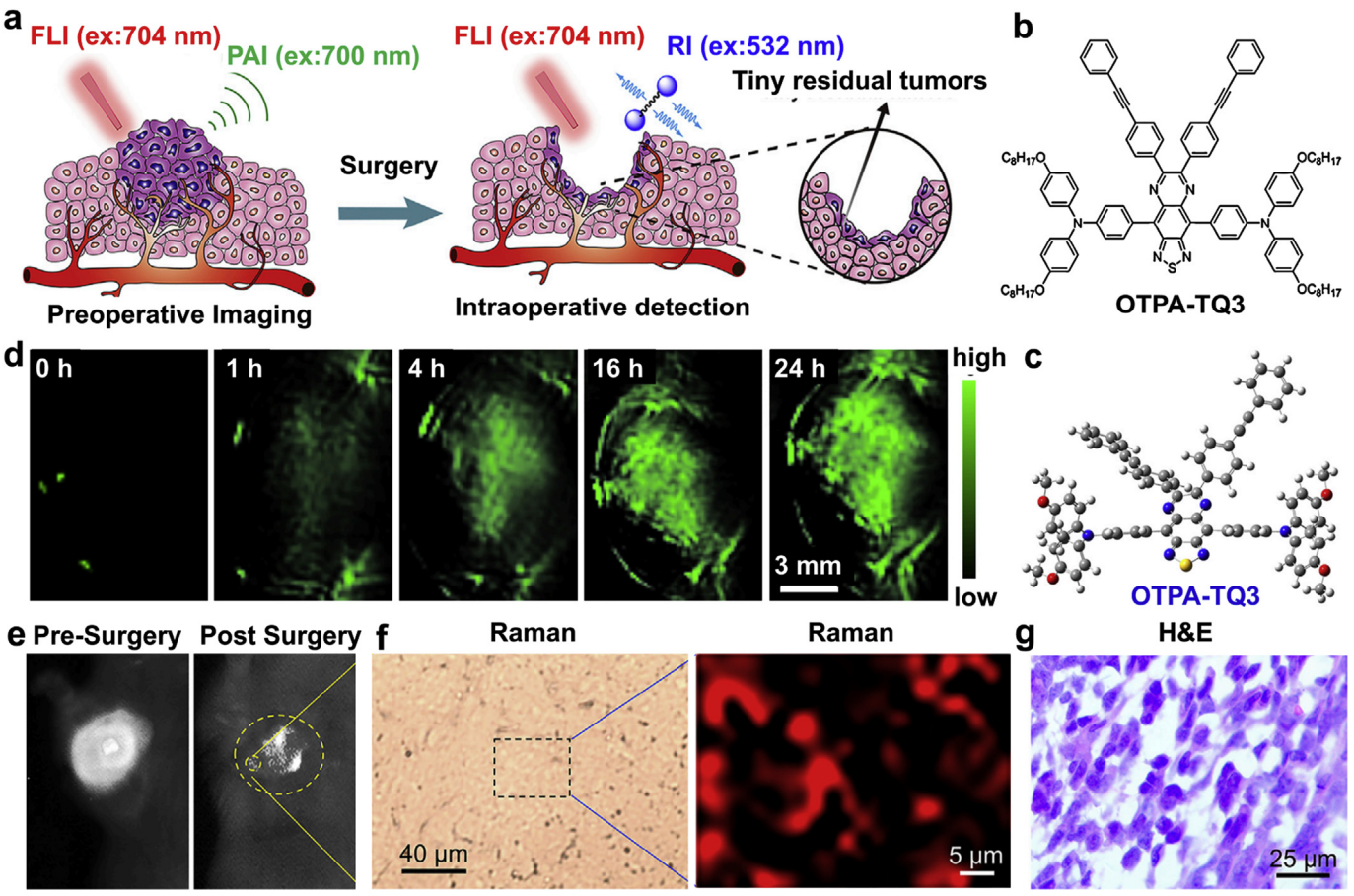

Fig. 5. (a) Schematic of cancer surgery with the help of three imaging modalities at different surgical stages. (b–c) Chemical structure and optimized molecular geometry of OTPA-TQ3. (d) Representative time-related PA images after iv injection of OTPA-TQ3 NPs before surgery. (e) Representative fluorescence images of the mice before and after surgery. (f) Raman imaging of doubtful resection site in e. (g) H&E stained sections make a definite diagnosis. (a–g) Adapted with permission from ref 21. Copyright 2019, Elsevier.

as strong intermolecular interactions led to luminescence quenching by large plane structures. This result demonstrated the advantages of iMAB in promoting afterglow luminescence by reducing the intermolecular interactions. Thereby, non-radiative decay was inhibited in AGL-AIE dots, and more energy can dissipate throw radiative pathway for optimized afterglow bioimaging. Furthermore, Ding and co-workers firstly applied afterglow imaging in the guidance of cancer resection using mouse models of peritoneal tumor metastases by system administration of AGL-AIE dots. It is worth mentioning that afterglow signals collected from AGL-AIE dots in mouse liver were nearly undetectable in the intraoperative image-guided cancer resection, which produced an ultrahigh tumor-to-liver ratio, and 100 times higher than that of fluorescence modality (Fig. 3e). With the help of afterglow imaging guidance, they completely removed the tiny nodules (diameter < 1 mm) that escaped from unguided surgery, provided a new opportunity to precise cancer surgery using iMAB.

4. Multi-modal image-guided surgery

Before cancer resection, comprehensive information of the lesions is needed to help surgeons make an accurate and reliable evaluation. Photoacoustic imaging (PAI) breaks through the centimeter depth limitation that constrained the optical bioimaging, highly promoting the presurgery diagnosis in preclinical studies [16,21,25]. Nevertheless, intraoperative cancer resection also requires the real-time guidance with ultrahigh sensitivity, which exactly can be met by fluorescence imaging (FLI). Thereby, PAI/FLI dual-modality of medical imaging are rapidly developing [31,48]. However, although there are many kinds of materials own PA/FL dual-modality, few of them can reach the maximal performance at each imaging modality, owing to the competitive energy pathway for PAI (non-radiative decay) and FLI (radiative pathway) at excited state. Inspired by tuning the molecular motions, Tang, Ding and co-workers designed a light-driven transformable molecule with PAI/FLI dual-modality for promoted cancer surgery [31]. This molecule named DTE-TPECM was designed with DTE as light-operated switch (UV/visible light) in the center and two TPECM groups as motion units on each side (Fig. 4a). In the ring-closed state (RClosed-DTE-TPECM), the non-radiative pathway was maximally optimized for PAI due to energy transfer from TPECM to closed DTE group and relatively strong intermolecular interactions such as π-π stacking (Fig. 4b). After visible light irradiation, this planar ring-closed molecule was transformed into ring-opened isomer (ROpen-DTE-TPECM) with twisted 3D structure for optimal FLI and ROS production, in which the non-radiative pathway was maximally inhibited by completely destroyed intramolecular energy transfer and intermolecular interactions (Fig. 4c). They further encapsulated the ring-closed molecules into nanoparticles using DSPE-PEG as matrix for promoted cancer surgery. This ring-closed nanoparticle that exhibited excellent PAI ability due to concentrate maximally harvested energy to non-radiative decay was intravenously injected into tumor-bearing mice for collecting deep information before surgery (Fig. 4d). During the resection surgery, operation area was irradiated with 610 nm red light to open the ring-closed molecules, thus boosting the FLI and ROS production by severe limitation of non-radiative decay. Under the guidance by FLI, tumor margins and residual submillimeter tumors could be clearly visualized and removed (Fig. 4e). Alternatively, if the completely resection was not recommended, the effective ROS

production of ROpen-nanoparticles can provide further treatment by PDT under light irradiation to prolong the survival time.

Multi-modality bioimaging benefits a lot to both pre-surgery diagnosis and intraoperative cancer resection by virtue of the advantages of each modality [21,49,50]. Taking the advantage of tuning the molecular structures and intramolecular motions, Tang, Ding and colleagues further designed a triple-modality molecule integrated FLI, PAI and Raman imaging (RI), followed by fabrication of nanoprobe to provide help in different surgical stages [21]. As shown in Fig. 5b-c, OTPA-TQ3 was synthesized with phenyl-alkyne-phenyl substitutes, alkoxysubstituted triphenylamine (OTPA) and thiadiazoloquinoxaline (TQ), featuring with twisted molecular structures and rich intramolecular motion units, which was encapsulated into nanoprobe with lipid-PEG_{2000} as the matrix. Pre-surgery diagnosis was performed by intravenous administration of this nanoprobe, including PAI and FLI, which were boosted by efficient intramolecular motions at excited state, twisted structures, strong AIE property and high absorption coefficient (Fig. 5d-e). Based on this diagnosis, intraoperative cancer resection was first conducted by an experienced surgeon with naked eyes. Then, under the FL imaging guidance, a few tiny residual tumors were clearly identified, meanwhile, further confirmation was made by RI with microscopic resolution (Fig. 5e-f). Noteworthy, 94% of Raman positive tiny tissues were real tumors based the analysis of H&E staining (Fig. 5g). In the assistant of this triple-modality surgery guidance in different stages, mouse survival rate was significantly promoted.

5. Summary and outlook

Intramolecular motion-associated biomaterials are developing fast due to the optimized bioimaging performance by regulation of their photophysical property, especially for intramolecular motions. Here, we summarized the recent progress in image-guided cancer surgery by virtue of optimized iMAB. Through inhibition of non-radiative decay by restriction of intramolecular motions and intermolecular interactions, the fluorescence performance of iMAB was optimized. In contrast, promoting the intramolecular motions or intermolecular interactions can highly concentrate the excited state energy on the non-radiative dissipation for excellent PAI. Smart molecular design as well as nanoengineering approach represent two different strategies for achieving the optimal imaging performance with iMAB. By introducing twisted structures and intramolecular motion units into the molecular design, we can easily inhibit the non-radiative decay for achieving maximal FL by restriction of molecular motions and intermolecular interactions such as π-π stacking. Alternatively, incorporation with other materials (e.g., calixarene, coranulene) that can provide confined interactions to restrict the intramolecular motions by nanoengineering method, also highly improves the FLI. In contrast, promoting the non-radiative decay by increasing the intramolecular motions or intermolecular interactions via smart chemical design/synthesis or nanoengineering approach, highly boosts the PAI.

As we known, cancer surgery is a comprehensive process including pre-surgery diagnosis and intraoperative resection. Pre-surgery diagnosis needs deep tissue penetration, which can be met well by PAI, while intraoperative resection requires ultrahigh sensitivity, which can be well-matched with FLI. Therefore, multi-modality imaging agents based iMAB can also be greatly beneficial to the different surgical stages by maximum effect of each modality via regulation of molecular motions. In this review, we summarized and discussed the regulation principles of iMAB for better performance in the field of image-guided cancer surgery. We hope more useful works in this field can be inspired by regulation of iMAB to promote the precise cancer surgery.

Declaration of competing interest

The authors declare no competing financial interests.

Acknowledgements

This work was supported by the National Natural Science Foundation of China (51873092 and 51961160730), the National Key R&D Program of China (Intergovernmental cooperation project, 2017YFE0132200), and the Fundamental Research Funds for the Central Universities, Nankai University.

References

[1] A. Kuellmer, J. Mueller, K. Caca, P. Aepli, D. Albers, B. Schumacher, et al., FTRD study group, Endoscopic full-thickness resection for early colorectal cancer, Gastrointest. Endosc. 89 (2019) 1180–1189.
[2] B.A. Whitson, S.S. Groth, S.J. Duval, S.J. Swanson, M.A. Maddaus, Surgery for early-stage non-small cell lung cancer: a systematic review of the video-assisted thoracoscopic surgery versus thoracotomy approaches to lobectomy, Ann. Thorac. Surg. 86 (2008) 2008–2018.
[3] E.Y. Lukianova-Hleb, Y.S. Kim, I. Belatsarkouski, A.M. Gillenwater, B.E. O'Neill, D.O. Lapotko, Intraoperative diagnostics and elimination of residual microtumours with plasmonic nanobubbles, Nat. Nanotechnol. 11 (2016) 525–532.
[4] C. Wang, Z. Wang, T. Zhao, Y. Li, G. Huang, B.D. Sumer, J. Gao, Optical molecular imaging for tumor detection and image-guided surgery, Biomaterials 157 (2018) 62–75.
[5] K.R. Tringale, J. Pang, Q.T. Nguyen, Image-guided surgery in cancer: a strategy to reduce incidence of positive surgical margins, WIREs Syst. Biol. Med. 10 (2018) e1412.
[6] C. Chi, Y. Du, J. Ye, D. Kou, J. Qiu, J. Wang, et al., Intraoperative imaging-guided cancer surgery: from current fluorescence molecular imaging methods to future multi-modality imaging technology, Theranostics 4 (2014) 1072–1084.
[7] M.R. Grootendorst, M. Cariati, A. Kothari, D.S. Tuch, A. Purushotham, Cerenkov luminescence imaging (CLI) for image-guided cancer surgery, Clin. Transl. Imag. 4 (2016) 353–366.
[8] T. Zhao, G. Huang, Y. Li, S. Yang, S. Ramezani, Z. Lin, et al., A transistor-like pH nanoprobe for tumour detection and image-guided surgery, Nat. Biomed. Eng. 1 (2017), 0006.
[9] J. Liu, C. Chen, S. Ji, Q. Liu, D. Ding, D. Zhao, et al., Long wavelength excitable near-infrared fluorescent nanoparticles with aggregation-induced emission characteristics for image-guided tumor resection, Chem. Sci. 8 (2017) 2782–2789.
[10] X. Gu, X. Zhang, H. Ma, S. Jia, P. Zhang, Y. Zhao, et al., Corannulene-incorporated AIE nanodots with highly suppressed nonradiative decay for boosted cancer phototheranostics *in vivo*, Adv. Mater. 30 (2018) 1801065.
[11] C. Chen, X. Ni, H. Tian, Q. Liu, D. Guo, D. Ding, Calixarene-based supramolecular AIE dots with highly inhibited nonradiative decay and intersystem crossing for ultrasensitive fluorescence image-guided cancer surgery, Angew. Chem. Int. Ed. (2020), https://doi.org/10.1002/anie.201916430.
[12] X. Ni, X. Zhang, X. Duan, H. Zheng, X. Xue, D. Ding, Near-infrared afterglow luminescent aggregation-induced emission dots with ultrahigh tumor-to-liver signal ratio for promoted image-guided cancer surgery, Nano Lett. 19 (2019) 318–330.
[13] X. Zhang, C. Li, W. Liu, H. Ou, D. Ding, Surface-adaptive nanoparticles with near-infrared aggregation-induced emission for image-guided tumor resection, Sci. China Life Sci. 62 (2019) 1472–1480.
[14] S. Zhu, R. Tian, A.L. Antaris, X. Chen, H. Dai, Near-infrared-II molecular dyes for cancer imaging and surgery, Adv. Mater. 31 (2019) 1900321.
[15] P. Wang, Y. Fan, L. Lu, L. Liu, L. Fan, M. Zhao, et al., NIR-II nanoprobes in-vivo assembly to improve image-guided surgery for metastatic ovarian cancer, Nat. Commun. 9 (2018) 2898.
[16] L.V. Wang, S. Hu, Photoacoustic tomography: *in vivo* imaging from organelles to organs, Science 335 (2012) 1458–1462.
[17] C. Xie, X. Zhen, Q. Miao, Y. Lyu, K. Pu, Self-assembled semiconducting polymer nanoparticles for ultrasensitive near-infrared afterglow imaging of metastatic tumors, Adv. Mater. 30 (2018) 1801331.
[18] Y. Jiang, J. Huang, X. Zhen, Z. Zeng, J. Li, C. Xie, et al., A generic approach towards afterglow luminescent nanoparticles for ultrasensitive *in vivo* imaging, Nat. Commun. 10 (2019) 2064.
[19] J. Yang, X. Zhen, B. Wang, X. Gao, Z. Ren, J. Wang, et al., The influence of the molecular packing on the room temperature phosphorescence of purely organic luminogens, Nat. Commun. 9 (2018) 840.
[20] Z. Zhao, C. Chen, W. Wu, F. Wang, L. Du, X. Zhang, et al., Highly efficient photothermal nanoagent achieved by harvesting energy via excited-state intramolecular motion within nanoparticles, Nat. Commun. 10 (2019) 768.
[21] J. Qi, J. Li, R. Liu, Q. Li, H. Zhang, J.W.Y. Lam, et al., Boosting fluorescence-photoacoustic-Raman properties in one fluorophore for precise cancer surgery, Inside Chem. 5 (2019) 1–21.
[22] Y. Ju, B. Dong, J. Yu, Y. Hou, Inherent multifunctional inorganic nanomaterials for imaging-guided cancer therapy, Nano Today 26 (2019) 108–122.
[23] Y. Sun, M. Ding, X. Zeng, Y. Xiao, H. Wu, H. Zhou, et al., Novel bright-emission small-molecule NIR-II fluorophores for *in vivo* tumor imaging and image-guided surgery, Chem. Sci. 8 (2017) 3489–3493.
[24] D. Ghosha, A.F. Bagleya, Y.J. Nae, M.J. Birrere, S.N. Bhatiaa, A.M. Belcher, Deep, noninvasive imaging and surgical guidance of submillimeter tumors using targeted M13-stabilized single-walled carbon nanotubes, Proc. Natl. Acad. Sci. U.S.A. 111 (2014) 13948–13953.

[25] K. Pu, A. Shuhendler, J.V. Jokerst, J. Mei, S.S. Gambhir, Z. Bao, et al., Semiconducting polymer nanoparticles as photoacoustic molecular imaging probes in living mice, Nat. Nanotechnol. 9 (2014) 233–239.
[26] S. Liu, X. Zhou, H. Zhang, H. Ou, J.W.Y. Lam, Y. Liu, et al., Molecular motion in aggregates: manipulating TICT for boosting photothermal theranostics, J. Am. Chem. Soc. 141 (2019) 5359–5368.
[27] C. Chen, H. Ou, R. Liu, D. Ding, Regulating the photophysical property of organic/polymer optical agents for promoted cancer phototheranostics, Adv. Mater. 31 (2019) 1806331.
[28] S. Liu, C. Chen, Y. Li, H. Zhang, J. Liu, R. Wang, et al., Constitutional isomerization enables bright NIR-II AIEgen for brain-inflammation imaging, Adv. Funct. Mater. 30 (2019) 1908125.
[29] C. Chen, X. Ni, S. Jia, Y. Liang, X. Wu, D. Kong, et al., Massively evoking immunogenic cell death by focused mitochondrial oxidative stress using an AIE luminogen with a twisted molecular structure, Adv. Mater. 31 (2019) 1904914.
[30] Y. Gong, G. Chen, Q. Peng, W. Yuan, Y. Xie, S. Li, et al., Achieving persistent room temperature phosphorescence and remarkable mechanochromism from pure organic luminogens, Adv. Mater. 27 (2015) 6195–6201.
[31] J. Qi, C. Chen, X. Zhang, X. Hu, S. Ji, R.T.K. Kwok, et al., Light-driven transformable optical agent with adaptive functions for boosting cancer surgery outcomes, Nat. Commun. 9 (2018) 1848.
[32] A.L. Vahrmeijer, M. Hutteman, J.R. van der Vorst, C.J.H. van de Velde, J.V. Frangioni, Image-guided cancer surgery using near-infrared fluorescence, Nat. Rev. Clin. Oncol. 10 (2013) 507–518.
[33] G.M. van Dam, G. Themelis, L.M.A. Crane, N.J. Harlaar, R.G. Pleijhuis, W. Kelder, et al., Intraoperative tumor-specific fluorescence imaging in ovarian cancer by folate receptor-α targeting: first in-human results, Nat. Med. 17 (2011) 1315–1319.
[34] A.A. Potapov, S.A. Goryaynov, V.A. Okhlopkov, L.V. Shishkina, V.B. Loschenov, T.A. Savelieva, et al., Laser biospectroscopy and 5-ALA fluorescence navigation as a helpful tool in the meningioma resection, Neurosurg. Rev. 39 (2016) 437–447.
[35] S. Zhu, R. Tian, A.L. Antaris, X. Chen, H. Dai, Near-infrared-II molecular dyes for cancer imaging and surgery, Adv. Mater. 31 (2019) 1900321.
[36] J.B. Grimm, B.P. English, H. Choi, A.K. Muthusamy, B.P. Mehl, P. Dong, et al., Bright photoactivatable fluorophores for single-molecule imaging, Nat. Methods 13 (2016) 985–988.
[37] Z. Zhao, P. Lu, J.W.Y. Lam, Z. Wang, C.Y.K. Chan, H.H.Y. Sung, et al., Molecular anchors in the solid state: restriction of intramolecular rotation boosts emission efficiency of luminogen aggregates to unity, Chem. Sci. 2 (2011) 672–675.
[38] Y. Hong, J.W.Y. Lam, B. Tang, Aggregation-induced emission, Chem. Soc. Rev. 40 (2011) 5361–5388.
[39] Y. Hong, J.W.Y. Lam, B. Tang, Aggregation-induced emission: phenomenon, mechanism and applications, Chem. Commun. (2009) 4332–4353.
[40] D. Ding, K. Li, B. Liu, B. Tang, Bioprobes based on AIE fluorogens, Acc. Chem. Res. 46 (2013) 2441–2453.
[41] J. Du, S. Liu, P. Zhang, H. Liu, Y. Li, W. He, et al., Highly stable and bright NIR-II AIE dots for intraoperative identification of ureter, ACS Appl. Mater. Interfaces 12 (2020) 8040–8049.
[42] Y. Lyu, Y. Fang, Q. Miao, X. Zhen, D. Ding, K. Pu, Intraparticle molecular orbital engineering of semiconducting polymer nanoparticles as amplified theranostics for *in vivo* photoacoustic imaging and photothermal therapy, ACS Nano 10 (2016) 4472–4481.
[43] C. Xie, P.K. Upputuri, X. Zhen, M. Pramanik, K. Pu, Self-quenched semiconducting polymer nanoparticles for amplified *in vivo* photoacoustic imaging, Biomaterials 119 (2017) 1–8.
[44] C. Xie, X. Zhen, Q. Miao, Y. Lyu, K. Pu, Self-assembled semiconducting polymer nanoparticles for ultrasensitive near-infrared afterglow imaging of metastatic tumors, Adv. Mater. 30 (2018) 1801331.
[45] D. Cui, C. Xie, J. Li, Y. Lyu, K. Pu, Semiconducting photosensitizer-incorporated copolymers as near-infrared afterglow nanoagents for tumor imaging, Adv. Healthc. Mater. 7 (2018) 1800329.
[46] O. Green, S. Gnaim, R. Blau, A. Eldar-Boock, R. Satchi-Fainaro, D. Shabat, Near-infrared dioxetane luminophores with direct chemiluminescence emission mode, J. Am. Chem. Soc. 139 (2017) 13243–13248.
[47] K.J. Bruemmer, O. Green, T.A. Su, D. Shabat, C.J. Chang, Chemiluminescent probes for activity-based sensing of formaldehyde released from folate degradation in living mice, Angew. Chem. Int. Ed. 57 (2018) 7508–7512.
[48] W. Tang, W. Fan, J. Lau, L. Deng, Z. Shen, X. Chen, Emerging blood-brain-barrier-crossing nanotechnology for brain cancer theranostics, Chem. Soc. Rev. 48 (2019) 2967–3014.
[49] K. Yang, L. Hu, X. Ma, S. Ye, L. Cheng, X. Shi, et al., Multimodal imaging guided photothermal therapy using functionalized graphene nanosheets anchored with magnetic nanoparticles, Adv. Mater. 24 (2012) 1868–1872.
[50] D. Huang, S. Lin, Q. Wang, Y. Zhang, C. Li, R. Ji, et al., An NIR-II fluorescence/dual bioluminescence multiplexed imaging for *in vivo* visualizing the location, survival, and differentiation of transplanted stem cells, Adv. Funct. Mater. 29 (2019) 1806546.
[51] V.J. Pansare, S. Hejazi, W.J. Faenza, R.K. Prud'homme, Review of long-wavelength optical and NIR imaging materials: contrast agents, fluorophores, and multifunctional nano carriers, Chem. Mater. 24 (2012) 812–827.
[52] M. Liong, J. Lu, M. Kovochich, T. Xia, S.G. Ruehm, Andre E. Nel, et al., Multifunctional inorganic nanoparticles for imaging, targeting, Drug Deliv. 2 (2008) 889–896.
[53] Kai Li, Bin Liu, Polymer-encapsulated organic nanoparticles for fluorescence and photoacoustic imaging, Chem. Soc. Rev. 43 (2014) 6570–6597.